Synthesis, Characterization, and Optical Properties of Titano-Molybdenum Phosphate Glasses

H. Es-soufi[1,2] · L. Bih[1,3]

Abstract

Melt quenching was used to prepare glasses of the $20Na_2O–(40–x)$ $Na_2MoO_4–xTiO_2–40P_2O_5$ system ($0 \leq x \leq 10$ mol.%). Xray diffraction and thermal analysis by differential scanning calorimetry (DSC) were utilized to check for possible crystalline residues and the glassy state. Structural characterizations of these prepared glasses were realized by density, molar volume, and glass transition temperature (T_g). The data collected from the parameters of density and T_g showed that their values depend on the glassy composition. Raman and infrared (IR) spectroscopies were used to investigate structural characterization. The compositions contain more water-resistant $PO_3^{2-}(Q^1)$ and $PO_4^{3-}(Q^0)$ units, according to glass durability testing. Using optical measurements, some parameters, such as optical band gap (E_g) and Urbach energy (ΔE), have been evaluated. These parameters were developed in the opposite sense, where E_g decreased from 2.35 to 1.85 eV and ΔE increased from 0.42 to 0.52 eV. This variation is associated with the production of non-bridging oxygens depending on the insertion of TiO_2 into glasses. Also, other parameters are determined by the UV-Visible absorption, and optical basicity (A_{th}), electronic polarisability (α_{O2-}), and electronegativity ($\Delta\chi^*$) are decreased, respectively, from 0.9244 to 0.8877 eV, from 1.9976 to 1.9670 eV, and from 0.8064 to 0.7634 eV with an increase of TiO_2 mol.%.

Graphical Abstract
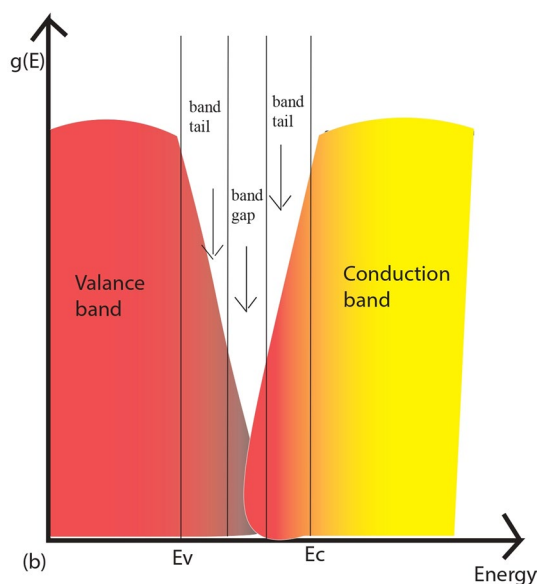
Keywords Phosphate glasses · IR spectroscopy · Raman spectroscopy · band gap · optical basicity · electronic polarizability · electronegativity

Extended author information available on the last page of the article

Introduction

The development of renewable energy sources such as wind, solar, and nuclear energy sources has had great advancement thanks to the continuation of research in this field. The imperative on this subject is associated with the limited availability of fossil fuel resources.[1] However, because the sources are variable, the disposal of these renewable sources cannot guarantee a consistent power supply. For this reason, researchers are focusing their efforts on energy storage to manage the intermittent nature of energy sources. Discovering rechargeable batteries that can store chemical energy and switch it into electrical energy with high efficiency has become an urgent necessity.[2] Like a typical rechargeable electrochemical battery, lithium-ion batteries depend on their high output voltages, high energy densities, and long cycle lives. Therefore, they have been widely used on the market for portable electronic devices, electric vehicles, etc. However, the high cost and the shortage of lithium resources are discouraging the application of Li-ion batteries in large-scale energy storage.[3–6] But Na-ion batteries are one promising alternative to the second-generation batteries to replace the commercial Li-ion batteries, because of their low price, abundant sodium resources, and high-level safety.[7–10]

In comparison with the Li atom, the Na atom is heavier and larger. However, the gravimetry and energy density of the Na-ion batteries does not exceed those of the Li-ion batteries.[11] Nevertheless, energy density is not a critical issue in the field of large-scale grid support. On the contrary, it considers operating costs and battery durability as important aspects.[12,13] In the context of this subject, many scientists have been interested in finding good materials made of crystal, glass, and/or glass-ceramic, despite their different components.[14–16] These prepared materials may be used as anodes, cathodes, or electrolytes.[17]

In focusing on glassy materials, many publications reported that the phosphate glasses functioned like cathodes or electrolytes.[15,18] Some perspectives in the area of the phosphate materials applied to Na-ion batteries are also deeply discussed.[19] Phosphate materials are ambitious in applying them as electrodes for energy storage.[20] Furthermore, phosphate glasses generally have poor durability in aqueous solutions.[21–24] But the addition of some transition elements (Mo, Ti, Fe) to phosphate glasses enhances their chemical durability, according to the desired application. Raman and ^{31}P magic angle spinning–nuclear magnetic resonance (^{31}P–MAS–NMR) data from molybdenum phosphate glasses showed that molybdenum ions occupy the modifying sites. In the glass framework, the metaphosphate chains are converted into pyrophosphate (PO_3^{2-}) and orthophosphate (PO_4^{3-}) chains.[25,26] In calcium phosphate

glasses, the MoO_3 content plays a role as the network modifier or network co-former, according to its concentration. When MoO_3 mol.% is less than 1 mol.%, the metaphosphate chains (Q^2) are dominant. If MoO_3 mol.% is between 5 and 10 mol.%, Q^2 units are reduced into Q^1 units, and if MoO_3 content is higher than 20 mol.%, the Mo atoms create their own MoO_6 units.[27] Most studies of molybdophosphate glasses are interested in the resist-solution of these glassy materials. The Al_2O_3–(or Fe_2O_3)–MoO_3–P_2O_5 systems are used to make iron or aluminum molybdophosphate glasses[28] where physicochemical properties such as glass transition temperature (T_g), viscosity, and solubility in water have been measured. In addition, the optical and electron spin resonance (ESR) data of molybdenum borophosphate glasses confirmed that molybdenum ions coexist in two states: Mo^{5+} and Mo^{6+}. In addition, electron hopping between these molybdenum ions leads to electronic conduction.[29]

The incorporation of titanium dioxide (TiO_2) with MoO_3 into a glassy phosphate system improves the chemical properties of the phosphate glasses. Researchers have recently expressed interest in the effects of TiO_2 mol.% on the chemical durability of glasses in the $20Li_2O$–($40-x$)Li_2MoO_4–$xTiO_2$–$40P_2O_5$ ($0 \leq x \leq 10$ mol.%) system.[30] In this work, we report an increase of TiO_2 mol.%, which leads to improved chemical durability. In another similar study, when MoO_3 was added to phosphate glasses containing iron, T_g and the aqueous dissolution rate were increased.[31] To the best of our knowledge, titanium in phosphate glasses generally exists in two forms: Ti^{4+} ions (a colorless to pale yellow color) and trivalent Ti^{3+} (a purple color). This latter form exhibits two electronic transitions, as $^2B_{2g} \rightarrow ^2B_{1g}$ and $^2B_{2g} \rightarrow ^2E$. However, in previous work, the addition of titanium to the tungsten phosphate network did not show any optical absorption depending on the electronic transition of Ti^{3+} ions.[32] Most studies are interested in phosphate glasses containing titanium ions. They are focused on structural investigations and the contribution of Ti ions to strong chemical durability enhancing properties, in addition to optical properties.[33] Recently, many researchers have been interested in enhancing the chemical durability of alkali phosphate glasses by adding different metal oxides of the highest valence cations. Phosphate glasses that contain molybdenum are suitable candidates for potential applications in integrated micro-batteries and solid cathodes.[15]

The goal of this present work is to report the prepared alkaline phosphate glasses containing two metal oxides (Ti and Mo), to investigate their structural characterization and chemical durability. The synthesized glasses will be used as cathodes in the Na-ion batteries in the study. This paper focused on the addition of TiO_2 into sodium molybdenum phosphate glasses to obtain stable materials that have mixed ionic-electronic conductivity. In addition, the structure of

the elaborated glasses was studied by infrared and Raman spectroscopies. An ultraviolet-visible (UV-Visible) study is suggested to analyze the combination of the two contributions: ionic conduction due to mobile sodium ions and electron hopping between Mo^{5+} and Mo^{6+} and/or between Ti^{3+} and Ti^{4+}.

Experimental

Sample Synthesis

A series of $20Na_2O–(40–x)Na_2MoO_4–xTiO_2–40P_2O_5$ glasses with TiO_2 content ranging from 0 to 10 mol.% are prepared. Melt quenching was used to create the $Na_2O–Na_2MoO_4–TiO_2–P_2O_5$ glasses from Aldrich Chemicals' reagent-grade sodium carbonate (Na_2CO_3), titanium dioxide (TiO_2), sodium molybdate Na_2MoO_4, and hydrogen ammonium phosphate ($NH_4H_2PO_4$). The mixture of raw materials, according to their percentages, was calcined into an alumina crucible and held at a maximum temperature of 600°C for 2 h to remove the ammonia (NH_3), water (H_2O), and carbon dioxide (CO_2). Afterward, the mixture was melted at 900°C under ambient air. Subsequently, the melt was poured into a preheated graphite mold. Thus, the prepared glasses are characterized by the blue color having been cooled to room temperature. The obtained samples are placed into a desiccator until testing to protect them from moisture.

Glass Characterization

The amorphous state of the prepared glasses was checked by x-ray diffraction (XRD) analysis. X–ray diffraction patterns of glass powder showed no peaks associated with the crystalline phase between 10° and 90° of the angular range (2θ). The density values (ρ) of the studied glasses were determined by the Archimedes method. At 22°C, diethyl orthophthalate is used as a suspension medium. The estimated density is ± 0.01 g/cm³. Molar volume (V_m) of glass is calculated according to the formula $V_m = M/ρ$, where M is molar weight and ρ is the density of the corresponding glass. The relationship $OPD = \sum x_i n_i / V_m$ is used to calculate oxygen packing density (OPD), where x_i is the molar fraction of oxide $R_m O_n$ and n_i is the number of oxygen atoms in the studied oxide.[34]

Thermal analysis by differential scanning calorimetry (DSC) is employed for estimating glass transition temperature (T_g) and crystallization temperature (T_c) parameters. The obtained DSC curves correspond to ground glasses weighing around 42 mg by using an Evo analyzer (DSC131), with the heating rate fixed at 10°C/min. The temperature measurement error is about 2°C. The T_g values are determined as the onset temperature of the glass transition temperature range. A Fourier transform infrared (FTIR) TENSOR27 spectrometer was utilized for analysis of the structure of the prepared glasses in the 400–1400 cm⁻¹ frequency range at room temperature. IR spectra are determined from KBr pellets by using glass powder and KBr at a 1% ratio when forming compressed pellets. At ambient temperature, Raman analysis of the prepared glasses was recorded at the Horiba Jobin Yvon Lab Raman HR spectrometer. The Raman spectra were determined by backscattering geometry and excitation with He–Ne laser radiation (632.8 nm) at a power of 12 mW. Additionally, the exposure time was 3 s, the accumulated number was 10, and the spectral slit width was 1 mm.

Durability Testing

The chemical durability of the studied glasses was analyzed in line with their aqueous dissolution rate in demineralized water at about 25°C. The glasses are cut and polished into cube forms using SiC paper. Then, each glass was rinsed with acetone, dried at 120°C, and measured to calculate its exact surface area. Each block was placed into a bottle already full of distilled water with a pH of 6.8. The ratio of the surface area of polished glasses (S) depends on the volume of distilled water (V). The ratio was fixed at 0.02 (S/V = 0.02). All bottles were suspended in a thermostated bath full of water and kept at 30°C for 250 h. The aqueous dissolution rate, D_R, is determined from the equation $D_R = Dx/St$, where Dx is the mass loss (g), S is the sample surface (cm²) before the aqueous dissolution test, and t is the immersion time (h). The obtained pH values of the leaching solutions are measured by a pH meter.

Optical Measurements

For optical measurements of the prepared glasses, a UV-Visible spectrometer (Jasco V-570) was used with a barium sulfate ($BaSO_4$) plate as the standard (100% reflectance) for the ground glass. These measurements were used to establish optical parameters in the 200–1400-nm wavelength range at room temperature.

Optical Parameters: Band Gap (E_g), Urbach Energy (ΔE), Optical Electronegativity (Δχ*), Electronic Polarizability ($α_{O2-}$), and Optical Basicity ($Λ_{th}$)

There are two optical transitions that result in fundamental absorption. Davis and Mott describe these transitions with Eq. 1 for direct transitions[35]:

$$a(v) = B(hv - E_\gamma)^n \tag{1}$$

where B, E_g, and $h\nu$ are, respectively, band tailing, band gap, and the incident photon energy. n is an index and has two values, 2 and 1/2, for indirect allowed transitions and direct allowed transitions. Using the above two equations and plotting $(\alpha h\nu)^{1/2}$ and $(\alpha h\nu)^2$ as a function of photon energy ($h\nu$), one can find the optical energy band gap (E_{opt}) for indirect and direct transitions, respectively. This study considered amorphous semiconductors, which are differentiated by indirect transitions (n = 2). Therefore, the optical band gap is determined from Eq. 1 using n = 2 by extrapolation $(\alpha h\nu)^{1/2}$ as a function of the photon energy ($h\nu$).[35]

Urbach's law[36] is used to investigate UV-visible absorption data on the lower photon energy side. Equation 2 denotes the $\alpha(\nu)$ (absorption coefficient) in the following form:

$$\alpha(\nu) = B \exp(h\nu/\Delta E) \qquad (2)$$

where B is constant and E is the width of the band tails of the restricted states in the band gap. Duffy and Reddy et al. have established optical electronegativity according to Eq. 3[37]:

$$\Delta\chi^* = 0.2688 \times E_g \qquad (3)$$

where E_g is the optical band gap.

For the oxide glasses, the optical basicity is denoted by Eq. 4[38]:

$$\Lambda_{th} = \sum_i x_i A_i \qquad (4)$$

where x_i is the molar percentage of oxide i and A_i is the basicity of oxide i.

Also, optical basicity depends on the electronic polarizability of the oxygen ion (α_{o2-}). Duffy et al. suggested Eq. 5[39]:

$$\Lambda_{th} = 1.67 \left(1 - 1/\alpha_{O^2-}\right) \qquad (5)$$

Results

X-ray Diffraction Study

All prepared samples were subjected to x–ray diffraction (XRD) in the 10°–90° 2θ range. Figure 1a lists the XRD patterns of glassy samples. These x–ray patterns exhibit two broad diffusion scatterings observed at lower angles of 2θ between 15° and 40°. In addition, the x–ray patterns of all glasses were observed without any crystalline plane diffraction peaks, which confirms that all quenched powders have an amorphous characteristic.

Density and Molar Volume

As is well known, the density of glasses is strongly linked to the structure, molecular weight, and percentage of each oxide constituting the glass. The obtained values for the density of the glasses measured by the Archimedes method are gathered in Table I. These density values decreased from 3.88 g/cm^3 (x = 0) to 3.49 g/cm^3 (x = 10), as TiO$_2$ mol.% increased. In addition, the density values were investigated to determine the molar volume, as shown in Table I. In contrast, during the evolution of density, the values of molar volume increased from 40.70 cm^3 (x = 0) to 41.62 cm^3 (x = 10), with the addition of the TiO$_2$ content. Decreasing in density and increasing in molar volume depend on introducing the TiO$_2$ mol.% into the prepared glasses, as shown clearly in Fig. 1b.
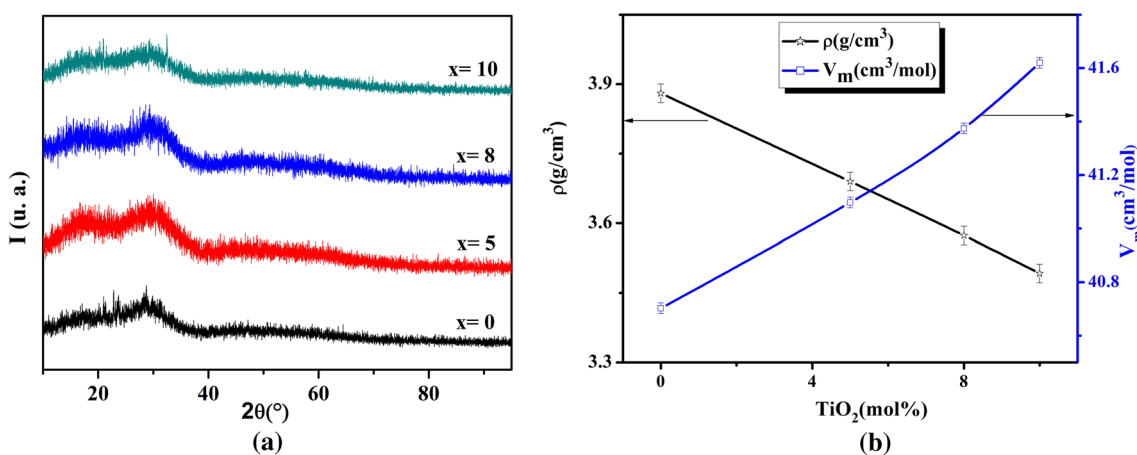

Fig. 1 (a) X-ray patterns of the Na$_2$O-Na$_2$MoO$_4$-TiO$_2$-P$_2$O$_5$ glasses; (b) composition dependence of the density and the molar volume for glasses.
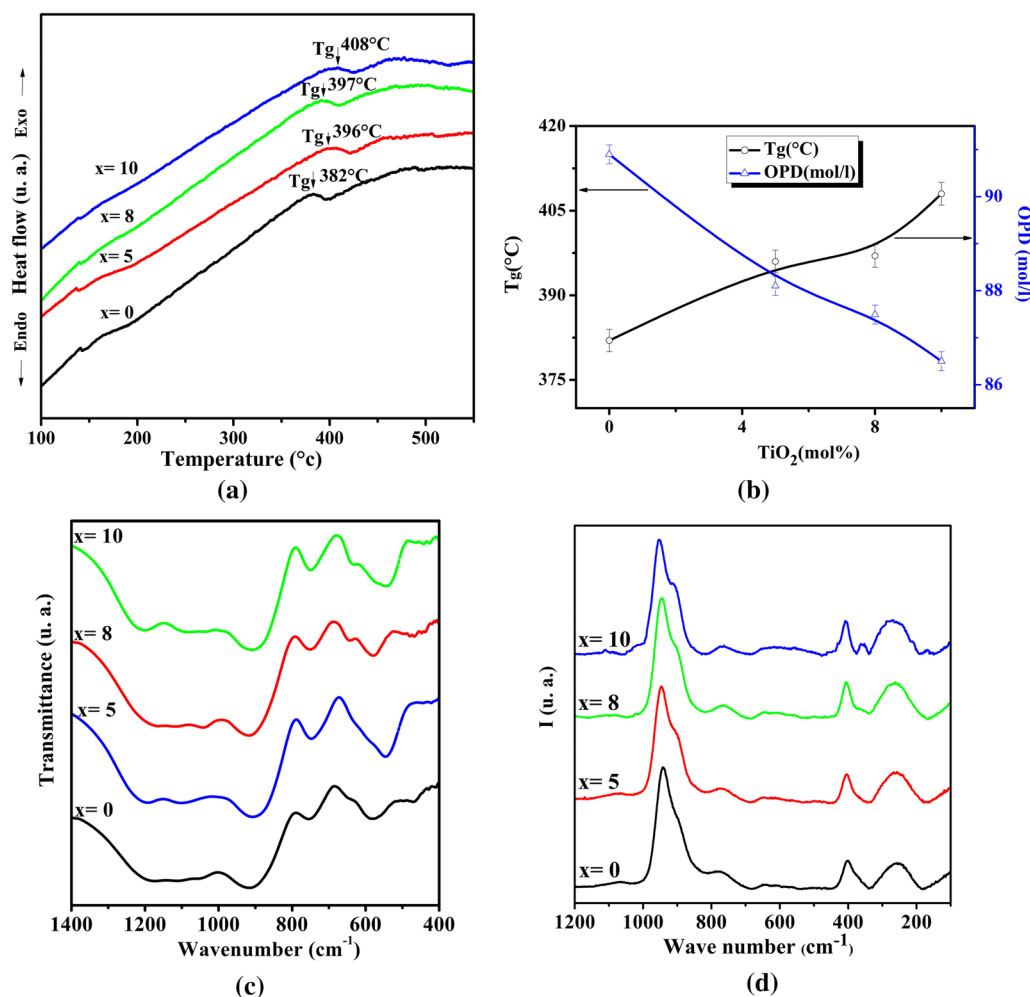
Fig. 2 (a) DSC thermograms of the studied glasses; (b) glass transition temperature (T_g) and oxygen packing density (OPD) of the studied glasses; (c) infrared spectra of the studied glasses; (d) Raman spectra of the studied glasses.

Differential Scanning Calorimetry (DSC) Results

Figure 2a shows DSC thermograms of glasses from the $20Na_2O$–$(40-x)$ Na_2MoO_4_$xTiO_2$_$40P_2O_5$ system. Also, Fig. 2b shows the dependence of T_g (glass transition temperature) on the addition of TiO_2 mol.%. The collected T_g results from DSC thermograms are gathered in Table I, where it is observed that T_g increased slowly from $382 \pm 4°C$ (x = 0) to $408 \pm 4°C$ (x = 10) with increasing TiO_2 content.

Fourier Transform Infrared (FTIR) Spectra

Infrared spectroscopy has been used to investigate the structure of the prepared glasses. The obtained data were interpreted into spectra, which were recorded in the frequency range of 1400–400 cm^{-1}, as shown in Fig. 2c. The

obtained spectra are based on the assignments of the different band positions as gathered in Table II. These assignments are made according to the literature for checking the phosphate units forming the glass framework.[16,40,41]

Raman Spectra

As shown in Fig. 2d, the Raman spectra of the $0Na_2O$– $(40-x)Na_2MoO_4$–$xTiO_2$–$40P_2O_5$ glasses (with $0 \leq x \leq 10$ mol.%) were recorded between 1200 and 150 cm^{-1}. These spectra are differentiated by bands, and their assignments are grouped in Table III. The following band positions were observed in the Raman spectra of the compositions (with x = 0, 5, 8, and 10 mol.%): 1120, 960, 900, 780, 400, and 250 cm^{-1}, where their assignments have been completed according to the literature.[16,42,43]
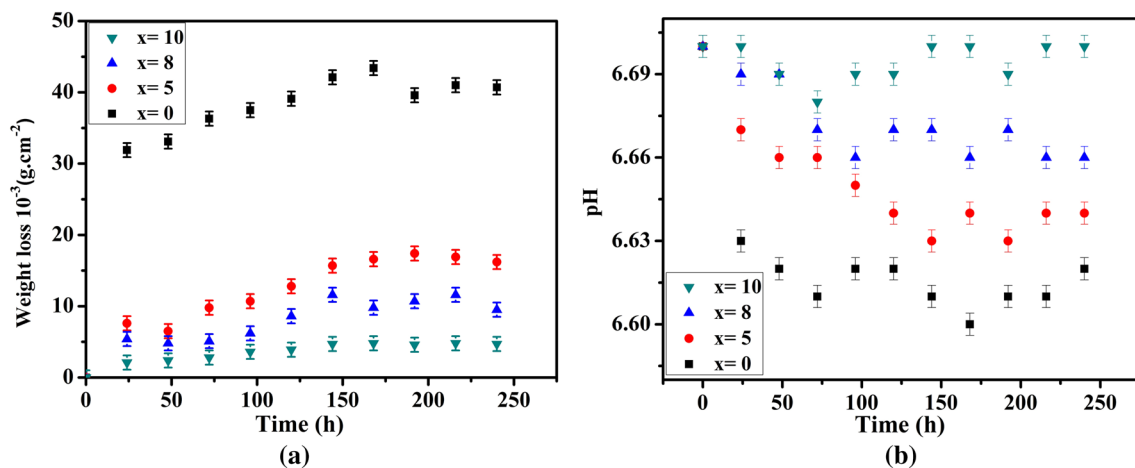
Fig. 3 (a) Evolution of the weight loss of the glasses as a function of immersion time (h); (b) Evolution of the pH of the glasses as a function of immersion time (h).

Chemical Durability

The studied glasses were submitted to durability test leaching 250 h. Every 24 h, the weight loss and pH of the leaching solution were measured. Figure 3a lists the evolution of weight loss with immersion time in the water. From this behavior, the curves of the aqueous dissolution rate have been observed in two regions: the first one is between 0 leaching hours and 150 leaching hours. It is characterized by increasing weight loss with immersion time. The second one is between 150 leaching hours and 250 leaching hours. It presents nearly plateau-like behavior. All glasses present the same behavior. However, there is a difference in the aqueous dissolution rate between the samples. Before 150 leaching hours, the glass of the composition x = 0 mol.% presented a higher weight loss than the other glasses of the composition x = 5, 8, and 10 mol.%. Figure 3b presents the curves of the evolution of pH as a function of immersion time (h). Also, all glasses present the same behavior, but there is an observed difference between these glasses. The evolution of pH curves also reveals two regions; the first one is between 0 leaching hours and 150 leaching hours, characterized by increasing pH. The second one is between 150 leaching hours and 250 leaching hours and has nearly linear behavior. In a comparison between the evolutions of aqueous dissolution curves and pH curves, it has been observed that there is a relationship between the aqueous dissolution rate and the pH of the leachate solution.

Ultraviolet–Visible Measurements

The treated glasses were analyzed by ultraviolet-visible (UV-Vis) spectroscopy in the 200–1400-nm wavelength range at room temperature. Figure 4a presents the curves of the studied glasses, which show a variation in the absorbance as a function of wavelength. These curves are differentiated by a strong and broad onset situated at 300 nm. Also, there is a weak broad bond in the 490–650-nm range.

Optical Parameters

The band gap (E_g) of the prepared glasses is determined by the Tauc method, from obtaining curves of the evolution of $(\alpha h\nu)^{1/2}$ as a function of $h\nu$ (eV), as gathered in Fig. 4b.[44] The obtained E_g values are shown in Table IV. As shown in Fig. 4c, the Urbach energy (ΔE) parameter is estimated from linear sections of the obtained curves by the evolution of the $\ln(\alpha)$ as a function of $h\nu$ (eV). The determinate values for Urbach energy (ΔE) are listed in Table IV. Duffy introduced the concept of optical electronegativity ($\Delta\chi^*$) as a concept to estimate many physical–chemical parameters that characterize materials.[39] Optical electronegativity is calculated in correlation with band gap energy. The obtained data are gathered in Table IV. Optical basicity (A_{th}) was evaluated to express the ability or power of an anion to share its electrons with surrounding cations.[38,45] The introduction of the concept of optical basicity is interesting for many applications.[46,47] In addition, optical basicity was originally obtained from the ultraviolet (UV) region of ions such as Pb^{2+} and Tl^+ dissolved as probes for sensing the electron donor power, oxygen.[40] Many macro- and microscopic physicochemical properties are known to influence electronic polarizability, including optical ultraviolet (UV) absorption of P block metal ions,[48] ionic refraction,[49–51] the electrooptical effect,[52] dielectric properties and ferroelectricity,[53,54] and chemical stability.[55,56] In addition, the electronic polarizability of the oxygen depends on ultraviolet transparency wavelengths, which are charge transfer bands of the
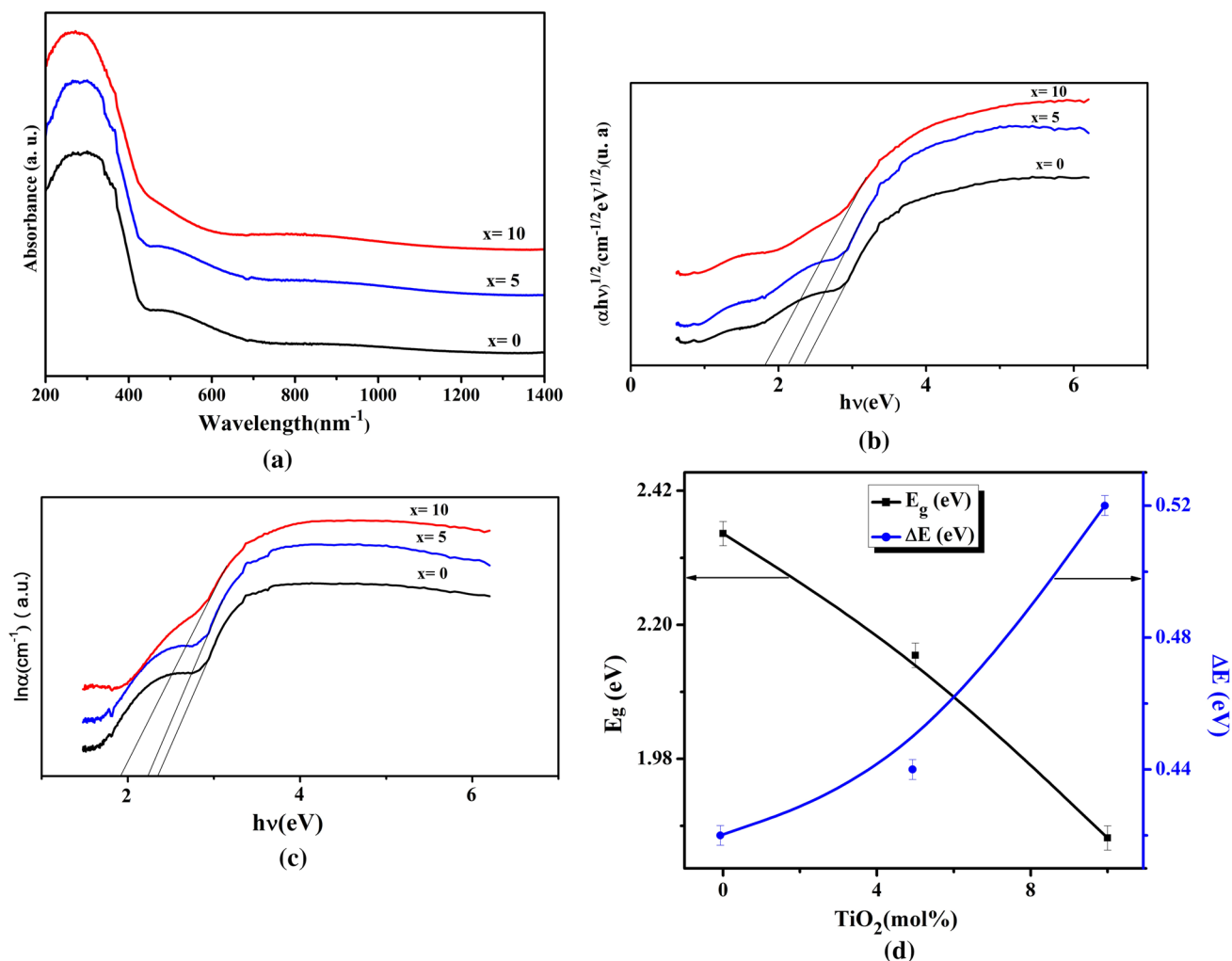
Fig. 4 (a) Optical absorption spectra of the prepared glasses; (b) Variation of $(\alpha h\nu)^{1/2}$ as a function of $(h\nu)$ for studied glasses; (c) Variation of $\ln(\alpha)$ as a function of $h\nu$ for the prepared glasses; (d) Evolution of band gap energy (eV) and Urbach energy (eV) as a function of TiO_2 mol.%.

dissolved metal ions. The magnitude of negative charges is narrowed by the oxide (II) species in glass and the basicity of glass. The determinate values of the electronic polarizability of the synthesized glasses are given in Table IV.

Discussion

Glass Forming and X-ray Patterns

At 900°C as the melting temperature, glasses of the $20Na_2O–(40–x)$ Na_2Mo_4_$xTiO_2$_$40P_2O_5$ system are prepared. The fraction (x = 0 mol.%) is the starting compound, and (x = 10 mol.%) is the limiting compound. The obtained samples were characterized by a blue color, which indicates the presence of reduced species (Mo^{5+} and/or Ti^{3+}) in the glass network. Nagarjuna et al. designed molybdenum ions to exist mainly in the form of Mo^{6+} states in the

$LiF–MoO_3–P_2O_5$: Ag_2O glass network. The Ag_2O concentration increased. The color of the samples became intensely blue. This blue color is associated with the reduction of part of the molybdenum ions of Mo^{6+} to Mo^{5+} states.[57] It has been reported that the color of the $xTiO_2–20BaO–(80–x)$ P_2O_5 glasses is gradually changed from brown to blue, a color with an increase of TiO_2 mol.%.[42] This variation in color of these present glasses is ascribed to electron transitions from one energy level to another. In addition, this color explains the presence of Ti^{3+} in the glass network. Many parameters influenced the incorporation of reduced species (Ti^{3+} and/or Mo^{5+}) into phosphate glasses, including glass melting, glass matrix, temperature-time, and redox conditions during the melt-quenching of the glasses.[58,59] In this case, it is difficult to estimate the origin of the blue color, which is due to the reduction of ions (from Mo^{6+} to Mo^{5+} and/or from Ti^{4+} to Ti^{3+}). The reduction of these species produces electronic conductivity. For this reason, we

proceeded to estimate the origin of this electronic conductivity by UV-Visible measurements (see the optical measurements section). The amorphous state of the obtained samples was verified by x-ray diffraction. The obtained XRD patterns were exposed to two broad-band diffusions (see Fig. 1a) at low angles instead of sharp peaks (a characteristic of crystalline materials), which confirms the amorphous nature of the present samples. Therefore, these two broadband diffusions may be associated with intermediate-range order in the glass framework.[60]

Density and Molar Volume

To the best of our knowledge, density is associated with the coordination number of the atoms involved, atomic radii, molecular weight, compactness, cross-link density, and the dimensions of interstitial space. Therefore, it can be determined that the variations in the glass structure are due to compositional modifications in the glass framework. It was previously explained in our previous work that the difference in molecular weight between Li_2MO_4 (M = Mo, W) and TiO_2 causes a decrease in density with the addition of TiO_2 mol.%. When light molecules (TiO_2 = 79.89 g/mol) replace heavy ones (Li_2MoO_4 = 173.82 g/mol or Li_2WO_4 = 261.8 g/mol), the density is decreased.[30] This explanation is supported by this work on Na_2MoO_4 (205.9371 g/mol) and TiO_2 (79.89 g/mol).

Molar volume is an interesting physical property. It was investigated to determine the structural compactness of the glasses, the interstitial space between the polyhedral and polyhedral lengths of bonds of the glassy network, and interatomic spacing within the glass framework. In our previous studies, increasing molar volume at TiO_2 content replaces Li_2MO_4 (M = Mo, W) and is associated with a smaller number of atoms and increasing cross-link density. Also, the introduction of TiO_2 content into the glass network leads to the formation of the new P–O–Ti bonds, which replace a part of the P–O–P bonds. In addition, P–O–Ti bonds interconnect phosphate chains, which lead to the formation of non-bridging oxygen on phosphorus atoms in metaphosphate Q^2 units, which constitute diphosphate Q^1 units (see the next sections: thermal analysis, IR, Raman, chemical durability, and optical measurement). This work is interested in substituting Na_2MoO_4 with TiO_2 content and confirms the suggested hypothesis of increasing molar volume in previous works.[30,32] Ernoek et al.[61] explained the increase in molar volume and decrease in density in $xTiO_2$– (40–x)ZnO–50P_2O_5 glasses (above 3 TiO_2 mol.%) by increasing the number of Q^1 structural units. Furthermore, Ganguli et al. suggested that the Q^1 structural chains are more voluminous than the Q^2 structural units, which occurs with an increase in molar volume and a decrease in density.[62]

Thermal Analysis

The thermograms (Fig. 2a) of the 20Na_2O–(40–x)Na_2MoO_4–$xTiO_2$–40P_2O_5 glasses (0≤x≤10 mol.%) show that T_g increases as TiO_2 content is introduced into the glass framework. This increase in T_g depends on many parameters. As is well known, T_g depends on oxygen-packing density (OPD). However, in this present study, it was found that oxygen-packing density progresses in the opposite direction with the evolution of T_g as a function of the TiO_2 mol.% (see Fig. 2b). From this, oxygen packing density does not explain the increase in T_g. Cernosek et al., on the other hand, explained the increase of T_g in the $xTiO_2$–(40–x)ZnO–10Na_2O–50P_2O_5 (1≤x≤20 mol.%) by many parameters based on each section of increased T_g. In section I (initial step), an increase in T_g (up to x = 3) may be explained by replacing the weaker covalent Zn–O bonds (bond energy ≈ 250 Kj/mol) with stronger covalent Ti–O bonds (bond energy ≈ 665 KJ/mol). In other sections (II and III), the increasing T_g glasses with an increase of TiO_2 mol.% are ascribed to reduced mobility in the melt. In addition, strengthening of a structure may be associated with decreasing the content of polymeric metaphosphate.[61] Furthermore, Segawa et al. reported that an increase in T_g with the addition of TiO_2 is due to the distortion of the glass network, which is associated with the formation of a three-dimensional network of P–O–Ti linkages.[63] In our case, the increase in T_g with the addition of the TiO_2 content was not due to increasing bond strength in the glasses because replacing the weak Ti–O bonds (bond energy ≈ 666.5 kJ/mol[64]) with the strong Mo–O bonds (bond energy ≈ 748 kJ/mol[64]), T_g is decreased. As a result, it is reasonable to conclude that bond strength and oxygen-packing density parameters cannot explain the increase in T_g, as confirmed by our previous studies.[30,32] From this, it is concluded that the increase of T_g with the addition of the TiO_2 mol.% may depend on (1) cross-link density by TiO_x (x = 4 or 6) structural units formed in the glass framework[30,32]; (2) reducing mobility in the melt[61]; (3) decreasing the content of polymeric metaphosphate (see Raman and IR sections)[61]; and (4) distortion of the glass framework associated with forming the three-dimensional network of P–O–Ti linkage.[63]

Infrared Spectra

The asymmetric vibration stretching of the P=O bond (v_{as}(P=O) and/or v_{as}(PO$_2$)) in the Q^2 structural chains is responsible for the broadband of approximately 1220–1200 cm^{-1} in Fig. 2c.[65] The band at 1160 cm^{-1} is attributed to symmetric vibration modes v_s (PO$_2$), in the Q^2 groups.[66] A strong band at 1100 cm^{-1} distinguishes the asymmetric vibrations of the nas(PO$_3$)$^{2-}$ pyrophosphate units.[66] The band at about 1070 cm^{-1} may be

due to symmetric vibration modes of $(PO_3)^{2-}$ units.[67] The band at the 1040–1000 cm^{-1} position of the low-intensity shoulder can be ascribed to PO_4^{3-} orthophosphate structural units.[68] The asymmetric vibration of the P–O–P/P–O–M (M=Mo, Ti) bonds is associated with the bands at 970–930 cm^{-1}. The band at 730 cm^{-1} can be linked to the symmetric stretching vibration of the P–O–P vs(P–O–P) bonds of the bridging oxygens (BOs). The broadband located in the range between 670 and 480 cm^{-1} could be due to bending vibrations of the phosphate structural units. The band around 655 cm^{-1} is linked to the symmetric vibration of the bond P–O–P in Q^2 units. The band around 520 cm^{-1} may include the deformation modes of the PO_4 groups. Through the IR band assignments, it was observed that the structure of the studied glasses contains bonds of different phosphate groups such as metaphosphate (PO_2^-) Q^2 units, pyrophosphate (PO_3^{2-}) Q^1 units, and orthophosphate (PO_4^{3-}) Q^0 units. But there is no band situated at a position higher than 1300 cm^{-1}, associated with v(P=O) of Q^3 structural units.[69] As gathered in Fig. 2c, it appears that IR spectra have changed slightly with an increase in TiO_2 content. There appeared to be some changes in band position and intensity, from composition x= 5 mol.%. These changes could be dependent on the interaction of the $(40–x)Na_2O$ with $xTiO_2$ or/ and $(40–x)MoO_3$ with $xTiO_2$ mol.%. When MoO_4 (725 cm^{-1}) and $MoO6$ (923 cm^{-1}) units coexisted in glasses based on the P_2O_5 former, the IR spectra were characterized by the coexistence of the MoO_4 (725 cm^{-1}) and MoO_6 (923 cm^{-1}) units.[30] By increasing the TiO_2 mol.% in the glasses, the intensities of the bands about 1000 cm^{-1} associated with P–O–P symmetric stretching into the PO_4^{3-} groups and TiO_4 units decreased. In addition, band positions slightly shift towards lower wavenumbers. The bands at 640 cm^{-1} are associated with the Ti–O–Ti bonds of the TiO_4 and TiO_6 structural units.[70] It can be concluded that the introduction of the TiO_2 mol.% into the glass network leads to an increase in the intensity of the bands associated with the P–O–P bonds of the $(PO_2)^-$ metaphosphate structural units. But the intensity of the band may be attributed to the $(PO_3)^{2-}$ pyrophosphate structural groups, as it decreased.[71] The band that appeared at 795 cm^{-1} could be due to the P–O–M (M=Ti, Mo) rings. It shifts to a lower frequency at Na_2O, substituting the MoO_3 content. Therefore, the P–O–M (M = Ti, Mo) bonds could be interrupted by alkaline groups $(Li_2O, Na_2O, K_2O...)$.[72] Therefore, it can be assumed that the P–O–M (M= Ti, Mo) bonds may form the NaO_2 mol.%, which leads to the new P–O–Ti bonds.[30] The presence of the P–O–Ti bonds in the glass network can increase T_g, which was confirmed by thermal analysis.

Raman Spectra

Figure 2d shows many bands at different positions between 1200 and 100 cm^{-1}. Most bands are mainly assigned to bonds of the phosphate glass framework. Because of the symmetric $v_s(PO^{2-})$ vibration in Q^2 chains, there is a weak broadband near 1120 cm^{-1}.[30] The strong band located between 960 and 900 cm^{-1} may be attributed to the asymmetric vibration P–O–P in Q^1 pyrophosphate units. However, Choudari et al. observed a band around the position of 900 cm^{-1} in the Raman spectra of the $50Ag_2O–xMoO_3–(50–x)$ P_2O_5 glasses, which may be attributed to vibration of the O–Mo–O bonds of MoO_4 structural units.[73] In addition, Koudelka et al. reported that the band at the 898 cm^{-1} position is ascribed to the O–Mo–O bonds in the Raman spectrum of the Ag_2MoO_4 crystalline unit.[74] Es-soufi et al. designed a band in the 900–950 cm^{-1} region, which may be due to the stretching vibration modes of MoO_4 tetrahedra. The band at the 800–900 cm^{-1} region is due to the Mo–O–Mo stretching of coupled MoO_6 octahedra.[30] However, Cernosek et al. discovered that the band in the Raman spectra of $xTiO_2–(40–x)ZnO–10Na_2O–50P_2O_5$ glasses between 900 cm^{-1} and 930 cm^{-1} could be attributed to TiO_6 stretching modes. Also, the band at about 970 cm^{-1} could be ascribed to stretching modes of the P–O–Ti modes.[61] The band around 780 cm^{-1} could be associated with symmetric vibration modes of the P–O–P bonds into Q^1 pyrophosphate units. The band around 680 cm^{-1} may be associated with symmetrical vibration modes of the bridging oxygen (BOs) between the Q^2 structural units. The band at 400 cm^{-1} is associated with the Mo–O–P bonds. Finally, the band around 250 cm^{-1} may be due to deformation of the PO_4 phosphate tetrahedron.[75]

When the TiO_2 content in the $20Na_2O–(40–x)$ $Na_2MoO_4–xTiO_2–40P_2O_5$ glasses was increased from 5 to 10%, the intensity and position of the bands in the Raman spectra changed slightly. Cernosek et al. noted that with the increase of TiO_2 up to 3 mol.% and more, the intensity of the band at 1030 cm^{-1} was observed to be growing.[61] A weak band appears at 1025 cm^{-1} at x = 5 mol.% and is attributed to symmetric vibration modes of the non-bridging oxygen $(P_2O_7)^{4-}$ in Q^1 units.[76] The band at about 611 cm^{-1} was observed to shift to 630 cm^{-1} with an increase in TiO_2 mol.%, which can be associated with stretching modes of Ti–O bonds in TiO_6 octahedral groups. In addition, its intensity increases slightly with an increase in TiO_2 mol.%.[76] However, the intensity of the band around 680 cm^{-1} was observed to be nearly constant with an increase in TiO_2 content. From this, it can be suggested that the TiO_6 octahedra replace the MoO_6 octahedra in the glass framework because it has been observed that there is a big difference between the connectivity of the titanium and the molybdenum.[77] Furthermore, Brow et al. reported bands in the range
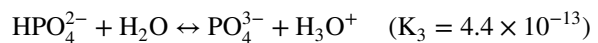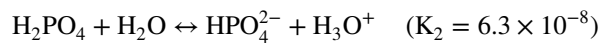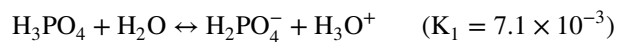
of 850–1300 cm^{-1} to form the Ti–O–P bonds with increasing TiO_2 content.[38] Furthermore, they noted that as TiO_2 increases in the glass network, metaphosphate units (Q^2) convert to pyrophosphate units (Q^1).[38] Also, Brauer et al. suggested that increasing TiO_2 content leads to creating more Q^1 units, and fewer Q^2 units can be associated with shorter phosphate chains, thus decreasing the connectivity of the glass network (see the section on optical parameters). In this context, Brauer et al. assumed that one TiO_2 converts two BOs (bridging oxygens) into four non-bridging oxygens (NBOs).[78]

Chemical Durability

Through the introduction of different metal oxides such as Al_2O_3, TiO_2, and Fe_2O_3 into glassy phosphate materials, one can change the chemical durability, biocompatibility, and other properties.[79–82] The purpose of this research was to determine the effect of TiO_2 mol.% on the chemical durability of phosphate glasses in the $20Na_2O$–$(40-x)$ Na_2MoO_4–$xTiO_2$–$40P_2O_5$ glasses. Figure 3a depicts the evolution of chemical durability as a function of immersion time (h). It observed two sections; the first one was up to 150 leaching hours. This section is distinguished by increasing the chemical durability, in addition to the TiO_2 content, in the glass network. This increase in chemical durability is associated with a decrease in hydration energy from Q^2 units to Q° units with the addition of the TiO_2 mol.%, which reduces Q^2 units into Q^1 and Q° units.[83] As is well known, the addition of TiO_2 content decreases glass solubility.[16,42] Brauer et al. suggested that titanium oxide (TiO_2) decreases the aqueous dissolution ratio of glasses because Ti^{4+} improved the cross-linking of phosphate chains related to Ca^{2+}, Mg^{2+}, and Na^+. However, TiO_2 lightly interrupts the glass network. Under the interruption effect, TiO_2 reduces the amount of Q^2 in Q^1 chains. Also, an increase in chemical durability could be associated with changes in bonds. When weaker P–O–(Li^+, Na^+) bonds and P=O bonds were combined with resistant P–O–Ti bonds, the number of covalent P–O–Ti bonds increased, resulting in improved hydrolytic resistance.[30] A second section, comprising between 150 leaching hours and 250 leaching hours, is connected to the saturation of the surrounding solution. This could be attributed to the number of covalent P–O–Ti bonds reaching their limit in the glass framework.

Several studies have attempted to control the degradability of phosphate glasses with titanium dioxide, which was demonstrated to be adequate for their improvement.[84–87] Also, their degradation can be controlled and fixed for varying times, from a few hours to many months, by altering the glass's chemistry.[85] The aqueous dissolution ratio of glasses is subjected to exchange reactions during the durability test. These reactions occur on glass surfaces between the ions (OH^- and H_3O^+) in water and the ions of the glass network, as follows[79]:

$$H_3PO_4 + H_2O \leftrightarrow H_2PO_4^- + H_3O^+ \quad (K_1 = 7.1 \times 10^{-3})$$

$$H_2PO_4 + H_2O \leftrightarrow HPO_4^{2-} + H_3O^+ \quad (K_2 = 6.3 \times 10^{-8})$$

$$HPO_4^{2-} + H_2O \leftrightarrow PO_4^{3-} + H_3O^+ \quad (K_3 = 4.4 \times 10^{-13})$$

Therefore, the exchange between ions that participate in the aqueous dissolution ratio of phosphate glasses determines the evolution of pH values. Figure 3b shows two sections of the evolution of the pH as a function of time immersion (h). The first one is limited to up to 150 leaching hours. The behavior of alterations occurs through sudden ion exchange between the phosphate glass framework and the surrounding solution.[79] The second one, occurring between 150 leaching hours and 250 leaching hours, could be due to saturation of the surrounding solution. This is related to the formation of protective layers or growth in forming the new P–O–Ti bonds. For this reason, diffusion into the surface of the phosphate glass framework has stopped. The relationship between the dissolution rate and the leachate pH is understandable as first the alkaline component (Na_2O) is dissolved. This is well known for the soda-lime glasses too.

Optical Absorption

As shown in Fig. 4a, the $20Na_2O$–$(40-x)$ Na_2MoO_4–$xTiO_2$–$40P_2O_5$ ($0 \leq x \leq 10$ mol.%) glasses have an ultraviolet (UV) absorption edge between 200 nm and 400 nm. The onset of the ultraviolet (UV) absorption band is about 300 nm. This absorption band could be due to traces of iron (Fe^{3+}) impurities in the raw materials or due to electron transitions between the state of the oxygen ions (2p) and the state of transition metal ions (3d).[88–91] It was observed that the host glass (x = 0) has a blue color, whereas the absorption spectrum of glassy composition x = 0 mol.% exhibits an absorption weak broadband located in the 490–650 nm region. In $47P_2O_5$–$24ZnO$–$(29-x)$ Na_2O–$xMoO_3$ ($0 \leq x \leq 10$) mol.% glasses with x = 2 mol.% MoO_3, Ibrahim et al. discovered two transmission bands in the 470–620 nm region. It was also discovered that all glasses contain MoO_3, which contains molybdenum in the form of Mo^{5+} and Mo^{6+} ions.[92] These apparent transmission bands in the visible region have been attributed to excitations of Mo^{5+} ($4d^1$) ions.[93] Goldstein et al.[94] explained the origin of two optical bands in glasses containing MoO_3 mol.% by excitations in Mo^{5+} ions, which can be caused by transitions from the b_2 (d_{xy}) ground state to (d_{xy}–d_{yz}) and (d_{x2}–d_{y2}) with E_1 = 15,000 cm^{-1} and E_2 = 23,000 cm^{-1}. Therefore, we can associate the weak absorption band situated between 490 and 650 nm with the

excitations of Mo^{5+} ($4d^1$) ions. Furthermore, at increasing concentration of TiO_2 in prepared glasses from 5 mol.%, it was observed that the blue color does not change. Furthermore, despite increasing the TiO_2 content up to 10%, the onset of UV absorption (300 nm) and the absorption band (490–650 nm) are nearly fixed. However, Toloman et al. studied ultraviolet–visible (UV–visible) absorption spectra of the $xTiO_2$–(1–x) [P_2O_5–CaO] glassy system (0.5<x<15 mol.%) in the 200–800 nm region, where, at an increase of TiO_2 mol.%, the onset of the absorption band around 318 nm shifts to the higher wavelength side. In addition to the exhibition, two optical absorption bands were associated with $^2B_{2g} \rightarrow ^2B_{1g}$ and $^2B_{2g} \rightarrow ^2A_{1g}$ transitions of the Ti^{3+} ion, respectively.[95] However, Kaur et al. reported that $50P_2O_5$–$5Al_2O_3$–20CaO–(25–x)Na_2O–$xTiO_2$ (0≤x≤12.5 mol.%) glasses have a purple color. This color is related to Ti^{3+} ions (d^1), which confirms the presence of a visible band (around 530 nm) attributed to $^3T_5 \rightarrow ^2T_3$ transition.[96]

Optical Parameters

Band Gap Energy (E_g) and Urbach Energy (ΔE)

From Table IV, it is observed that as TiO_2 mol.% increases in the glass network, the band gap (E_g) decreases from 2.35 eV (x = 0 mol.%) to 1.85 eV (x = 10 mol.%). A decrease in the value of E_g is due to the appearance of additional defect states in the glass framework.[97] As TiO_2 content enters into the glass network, bridging oxygens (BOs) are converted into non-bridging oxygens (NBOs). In addition, the NBOs have higher energy levels than the BOs. This conversion results in a reduction in band gap energy. As confirmed early by Raman and IR spectra, TiO_2 remains as a glass modifier and it occurs during the depolymerization of phosphate glass chains by converting Q^2 into Q^1 and $Q°$ structural units.[98]

Amorphous materials are characterized by disorder. This disorder results in the perturbation of the structural environment. As a result, the increase in NBOs leads to increasing disorder in the glass network. Furthermore, the disorder is evaluated by the Urbach parameter (ΔE).[99] From Table IV, the calculated values of the Urbach energy (ΔE) increased from 0.42 eV (x = mol.%) to 0.52 eV (x = 10 mol.%), as the TiO_2 content increased. In general, Urbach energy is used to estimate the degree of disorder in glassy structures. Furthermore, it is intended for glassy materials with a higher Urbach energy to convert their weak bonds into defects[100] when the Urbach energy values of the $50P_2O_5$–$5Al_2O_3$–20CaO–$20Na_2O$–$5TiO_2$ glasses (ΔE=0.362–0.128 eV) and the (95–x) TeO_2–$5La_2O_3$–$xTiO_2$ glasses (ΔE = 0.29–0.13 eV) were compared to the current glasses in the $20Na_2O$–(40–x) Na_2MoO_4–$xTiO_2$. In glassy materials, the structural

behavior (disorder) is also affected by TiO_2 mol.%.[99,101] From this, it can be concluded that the TiO_2 mol.% on a glass network depends on the composition of each material.

Figure 4d shows a correlation between band gap energy and Urbach energy, which is related to an increase in the TiO_2 mol.% in the glass network. From Fig.4d, it was observed that an increase in Urbach energy and a decrease in optical band gap energy were observed with increasing TiO_2 mol.%. This behavior may be attributed to an increase in the concentration of TiO_2 mol.% in the glass framework, which converts Q^2 into Q^1 and $Q°$ structural units. Thus, bridging oxygens (BOs) are converted to non-bridging oxygens (NBOs). Therefore, the optical band gap decreases and the Urbach energy increases. The evolution of the band gap and Urbach energy depends on the material nature (amorphous or crystal). In the literature, it has been reported that the band gap separates the valence band from the conduction band, as it relates to the nature of the studied material.[102] In crystal materials, the band gap between the conduction band and the valence band is perfectly defined by the quantity E_v–E_c. The distribution functions of energy state densities, g(E), are parabolic (Fig. 5a). For disordered materials, the band edges described in the crystal lattices and delimited by E_v and E_c can go as far as their disappearance. It was observed that the conduction band and valence band extend to the band gap. In addition, the presence of localized states within the band gap (existence of a certain non-zero density of the states within the gap) (Fig. 5b) can be encountered.

Electronegativity

The optical band gap value has a direct relationship with the width of the forbidden band. This latter depends on the intensity of electronic interactions between anions and cations of a given material. On the other hand, the band gap can be related to the difference in electronegativity (Δχ*) between interacting ions. From the values obtained for Δχ *, it was noted that electronegativity decreased with increasing TiO_2 content. This reduction concerns all the studied glasses, which decreases from 0.8064 to 0.7634 eV. From this, it was concluded that the addition of TiO_2 mol.% to glass reduces these Coulomb interactions between cations and oxygen ions, consequently leading to a decrease in electronegativity.[103] In addition, it found that the E_g decreased with increasing the Ti content as a result of increasing the non-bridging oxygens (NBOs) in the phosphate glasses. Therefore, increasing optical electronegativity could be associated with an increasing number of non-bridging oxygens (NBOs).
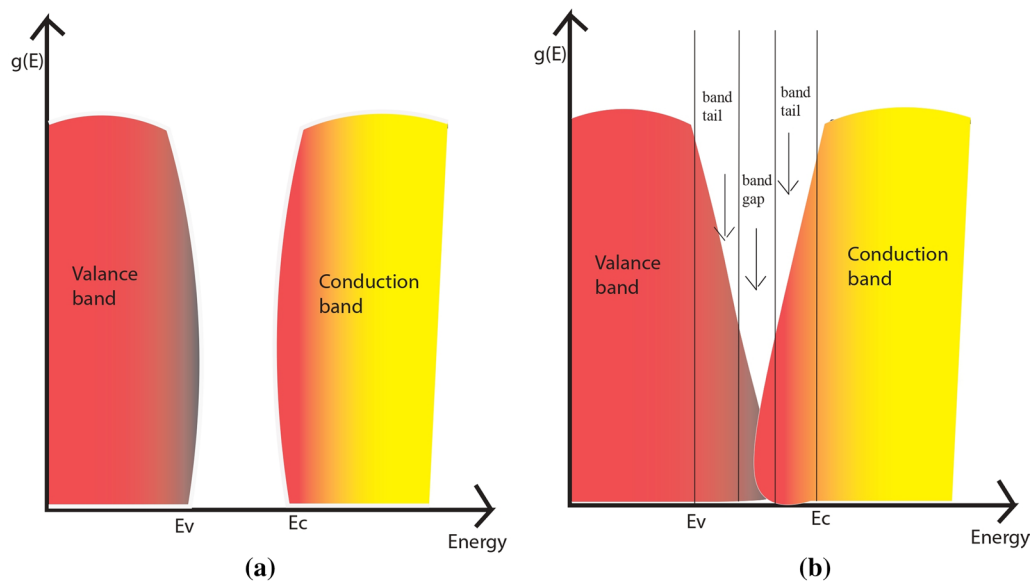
Fig. 5 Distribution functions of the densities of energy states g(E) in the bands for a crystalline semiconductor (a) and for a disordered material (b).

Table I Some physical properties for the studied glasses

x (mol.%)	Density ρ ($\pm 0.01 g/cm^3$)	Molar volume V_m (± 0.04 cm^3/mol)	Oxygen packing density (OPD) (mol/l)	Glass transition temperature T_g ($\pm 4°C$)
0	3.88	40.70	90.90	382
5	3.69	41. 10	88.10	396
8	3.57	41. 37	87. 49	397
10	3. 49	41.62	86.50	408

Table II IR band assignments in the 1400–400 cm^{-1} frequency range for the studied phosphate glasses

Position of band (cm^{-1})	Band assignment
1240	$\nu_{as}(P=O)/\nu_{as}(PO_2^-)$
1160	$\nu_s(PO_2)^-$
1100	$\nu_{as}(PO_3)^{2-}$
1000	$\nu_s(PO_4)^{3-}$
935–920	$\nu_{as}(P–O–P)/\nu_{as}(P–O–M)$ (M= Mo. Ti)
880–870	(M= Mo. Ti)
730	$\nu_s(P–O–P)$
640–630	$\nu_s(M–O–M)$ (M= Mo. Ti)
500–425	(O–P–O) and translation of cations

Table III Raman band assignments in the 1200–100 cm^{-1} frequency range for the studied phosphate glasses

Position of band (cm^{-1})	Band assignment
1120	$\nu_s(PO_2)^-$, Q^2
960	$\nu_{as}(P–O–P)/\nu_{as}(P–O–M)$ (M= Mo. Ti)
900	$O–Mo–O/MO_4/MO_6$ (M= Mo. Ti)
780	$\nu_s(P–O–P)$, Q^1
680	$\nu_s(P–O–P)$, Q^2
400	$\nu_s(M–O–M)$(M= Mo, Ti)
250	$\delta(PO_4)$

Theoretical Optical Basicity A_{th}

The estimated values of the theoretical optical basicity (Λ_{th}) are given in Table IV. The analysis of these values shows that optical basicity decreases from 0.9244 to 0.8877 eV, with an increase of TiO_2 mol.%. This decrease could be due to the

Mo^{5+}/Mo^{6+} ratio or another parameter (see the electronic polarizability section). Bih et al. discovered that the optical basicity of glasses containing $yLi_2O–0.05(MoO_3)_2–(0.95–y)$ P_2O_5 and $0.1Li_2O–0.9[x(MoO_3)_2–(1–x)P_2O_5]$ increased from 0.41 to 0.51 eV and from 0.41 to 0.43 eV, respectively. This increase in optical basicity may be due to a decrease in reduced species of molybdenum (Mo^{5+}).[59] Furthermore, molybdenum reduction in glasses could be attributed to a

Table IV Optical parameters of the fundamental optical band for the studied glasses

x (mol.%)	Optical band gap E_g(eV)	Urbach energy ΔE (eV)	Optical basicity A_{th} (eV)	Electronic polarizability α_{O2-} (eV)	Optical electronegativity $\Delta\chi^*$ (eV)
0	2.35	0.42	0.9244	1.9976	0.8064
5	2.15	0.44	0.8930	1.9731	0.7688
10	1.85	0.52	0.8877		0.7634

variety of factors, including glass composition, acid-base considerations (O^{2-} exchanges) associated with optical basicity, and complexation with O^{2-}.[59] As a result, increasing the non-bridging oxygens associated with increasing the TiO_2 mol.% is favored by increasing Mo^{5+}, thereby decreasing optical basicity.[104]

Electronic Polarizability

The estimated values of the electronic polarizability (α_{o2-}) of the synthesized glasses are gathered in Table IV. It is noted that α_{O2-} decreases from 1.9976 to 1.9670 eV when the concentration of TiO_2 increases. This variation can be related to the variation in the polarization of cations when one Na_2MoO_4 is substituted by TiO_2 content. Indeed, the substitution of a highly polarizable Mo^{6+} cation by a less-polarizable Ti^{4+} causes a decrease in electronic polarizability (α_{O2-}), which subsequently leads to a decrease in optical basicity.[105]

In this study, we were interested in phosphate glasses of the $20Na_2O–(40–x)Na_2MoO_4–xTiO_2–40P_2O_5$ system (where x = 0–10 mol.%), and it appears that these phosphate glasses are suitable materials for use as cathodes for sodium-ion batteries. The study confirmed this suggestion. The introduction of TiO_2 mol.% has created changes in a positive sense in glasses in the present study. By forming new P–O–Ti bonds from P–O–P and/or P=O bonds, as well as converting bridging oxygens (BOs) to non-bridging oxygens (NBOs), increasing the TiO_2 mol.% contributed to improved chemical durability. As a result, the Q^2 structural unit is converted to the Q^1 and $Q°$ structural units. Therefore, the ionic bonds increase in the glass framework. The addition of modifier oxides to glasses, as is well known, increases the non-bridging oxygens (NBOs) inside the glassy structure. Therefore, the modifier oxides occur as defects, which affect the physicochemical properties of glasses. Glasses containing various phosphate groups (PO_3^{2-} and PO_4^{3-}) and transition elements (Mo and Ti) were used to create the channels that shared the corners. Therefore, the presence of channels in the glass network helps sodium ions easily move through glassy materials. For this reason, our studied glasses are identified by their continuous open structure for the movement of ions, which helps in the random distribution of sodium carriers in the glass network. From

this, ionic conductivity can be obtained. Also, the hopping mechanism occurs between Mo^{5+} and Mo^{6+} cations. which leads to obtaining electronic conductivity. The coupling of these conductivities (ionic and electronic) leads to the achievement of mixed ionic–electronic conductor glasses. For this reason, it is expected that transition metal oxide glasses containing modifier ions can be utilized as stable cathode materials for sodium–ion batteries.

Conclusion

The $20Na_2O–(40–x)$ $Na_2MoO_4–xTiO_2–40P_2O_5$ ($0 \leq x \leq 10$ mol.%) glasses were the focus of our investigation. According to IR and Raman spectra, it was concluded that the addition of TiO_2 content into the glass network leads to the formation of the new P–O–Ti bonds. In addition, metaphosphate (PO^{2-}) Q^2 structural units are converted into pyrophosphate (PO_3^{2-}) Q^1 and orthophosphate (PO_4^{3-}) Q^0 structural units. Thanks to these changes in the glass network, water resistance has been improved. In addition, density with molar volume has been decreased and increased, respectively. Furthermore, the role of the Ti^{4+} ions is limited to structural changes in the studied glasses. While the reduced Ti^{3+} ions did not contribute to optical measurements, the reduced species Mo^{5+} ($4d^1$) were responsible for weak and broad absorption in the 490–650-nm range. The obtained values of the band gap (E_g) and Urbach energy (ΔE) show decreasing and increasing behavior, respectively. This behavior is based on increasing non-bridging oxygen (defects) inside the glass framework. Also, decreasing other optical parameters such as electronegativity ($\Delta\chi^*$), theoretical optical basicity (A_{th}), and electronic polarizability (α_{O2-}) are due to increasing non-bridging oxygens (NBOs). In the glass network, mixed ionic–electronic conductivity occurs due to the coexistence of the mobility of Na^+ ions (ionic conductivity) with the reduced species Mo^{5+} (electronic conductivity).

References

1. Z. Yang, J. Zhang, M.C. Kintner-Meyer, X. Lu, D. Choi, J.P. Lemmon, and J. Liu, Electrochemical energy storage for green grid. *Chem. rev.* 111, 3577 (2011). https://doi.org/10.1021/cr100290v.

2. M. Armand and J.-M. Tarascon, Building better batteries. *Nat.* 451, 652 (2008). https://doi.org/10.1038/451652a.

3. B. Dunn, H. Kamath, and J.-M. Tarascon, Electrical energy storage for the grid: a battery of choices. *Sci.* 334, 928 (2011). https://doi.org/10.1126/science.1212741.

4. J.B. Goodenough and K.-S. Park, The Li-ion rechargeable battery: a perspective. *J. Am. Chem. Soc.* 135, 1167 (2013). https://doi.org/10.1021/ja3091438.

5. M.S. Whittingham, Lithium batteries and cathode materials. *Chem. Rev.* 104, 4271 (2004). https://doi.org/10.1021/cr020731c.

6. J.B. Goodenough, How we made the Li-ion rechargeable battery. *Nat. Elec.* 1, 204 (2018). https://doi.org/10.1038/s41928-018-0048-6.

7. H. Kim, H. Kim, Z. Ding, M.H. Lee, K. Lim, G. Yoon, and K. Kang, Recent progress in electrode materials for sodium-ion batteries. *Adv. Energy Mater.* 6, 1600943 (2016). https://doi.org/10.1002/aenm.201600943.

8. S.W. Kim, D.H. Seo, X. Ma, G. Ceder, and K. Kang, Electrode materials for rechargeable sodium-ion batteries: potential alternatives to current lithium-ion batteries. *Adv. Energy Mater.* 2, 710 (2012). https://doi.org/10.1002/aenm.201200026.

9. S.V. Xiaocui Zhu, J.N. Savilov, L. Li, and L. Li, Carbon nano-flakes as a promising anode for sodium-ion batteries. *Funct. Mater. Lett.* 6, 1840011 (2018). https://doi.org/10.1142/S1793604718400118.

10. N. Yabuuchi, K. Kubota, M. Dahbi, and S. Komaba, Research development on sodiumion batteries. *Chem. Rev.* 114, 11636 (2014). https://doi.org/10.1021/cr500192f.

11. G.L. Xu, R. Amine, A. Abouimrane, H. Che, M. Dahbi, Z.F. Ma, I. Saadoune, J. Alami, W.L. Mattis, and F. Pan, Challenges in developing electrodes, electrolytes, and diagnostics tools to understand and advance sodium-ion batteries. *Adv. Energy Mater.* 8, 1702403 (2018). https://doi.org/10.1002/aenm.201702403.

12. H. Pan, Y.-S. Hu, and L. Chen, Room-temperature stationary sodium-ion batteries for large-scale electric energy storage. *Energy Environ. Sci.* 6, 2338 (2013). https://doi.org/10.1039/C3EE40847G.

13. F. Bella, F. Colo, J.R. Nair, and C. Gerbaldi, Photopolymer electrolytes for sustainable upscalable safe and ambient-temperature sodium-ion secondary batteries. *Chem. Sus. Chem.* 8, 3668 (2015). https://doi.org/10.1002/cssc.201500873.

14. M.S. Whittingham, Free energy of formation of sodium tungsten bronzes, NaxWO3. *J. Elect. Soc.* 122, 713 (1975).

15. S. Nakata, T. Togashi, T. Honma, and T. Komatsu, Cathode properties of sodium iron phosphate glass for sodium ion batteries. *J. Non-Cry. Sol.* 450, 109 (2016). https://doi.org/10.1016/j.jnoncrysol.2016.08.005.

16. H. Es-Soufi, L. Bih, A.R. Lima, A. El Bouari, B. Manoun, and S. Hussain, Investigation DSC and XRD on the crystallization kinetics in the phosphate Li₂O–Li₂WO₄–TiO₂–P₂O₅ glassy ionic system. *J Mat Sci Mater Elect* (2021). https://doi.org/10.1007/s10854-021-06804-7.

17. P. Jozwiak and J.E. Garbarczyk, Mixed electronic–ionic conductivity in the glasses of the Li₂O–V₂O₅–P₂O₅ system. *Sol. St. Ion.* 176, 2163 (2005). https://doi.org/10.1016/j.ssi.2004.06.028.

18. T. Uma, and M. Nogami, Influence of TiO₂ on proton conductivity in fuel cell electrolytes based on sol–gel derived P₂O₅–SiO₂ glasses. *J. Non-Cry. Sol.* 351, 3325 (2005). https://doi.org/10.1016/j.jnoncrysol.2005.08.010.

19. M. Ben Bechir and A. Ben Rhaiem, The sodium-ion battery: Study of alternative current conduction mechanisms on the Na₃PO₄ - Based solid electrolyte. *Phys. E* 120, 114032 (2020). https://doi.org/10.1016/j.physe.2020.114032.

20. Y. Liu, Y. Zhou, J. Zhang, S. Zhang, and P. Ren, The relation between the structure and electrochemical performance of sodiated iron phosphate in sodium-ion batteries. *J. Pow. Sour.* 314, 1 (2016). https://doi.org/10.1016/j.jpowsour.2016.03.003.

21. N.H. Ray, Composition–property relationships in inorganic oxide glasses. *J. Non-Crys. Sol.* 15, 423 (1974). https://doi.org/10.1016/0022-3093(74)90148-3.

22. J. Zarzycki, Les Verres et l'Etat Vitreux, Ed. Masson 1982

23. M.R. Reidmeyer, M. Rajaram, and D.E. Day, Preparation of phosphorus oxynitride glasses. *J. Non-crys. Sol.* 85, 186 (1986). https://doi.org/10.1016/0022-3093(86)90090-6.

24. H. Yung, P.Y. Shih, H.S. Liu, and T.S. Chin, Nitridation effect on properties of stannous-lead phosphate glasses. *J. Amer. Cer. Soc.* 80, 2213 (1997). https://doi.org/10.1111/j.1151-2916.1997.tb03110.x.

25. M. Szumera, Molybdenum modified phosphate glasses studied by 31P MAS NMR and Raman spectroscopy. *Spectrochim. Acta Mol. Biomol. Spectrosc.* 137, 111 (2015). https://doi.org/10.1016/j.saa.2014.08.038.

26. L. Koudelka, I. Rösslerová, J. Holubová, P. Mošner, L. Montagne, and B. Revel, Structural study of PbO–MoO₃–P₂O₅ glasses by Raman and NMR spectroscopy. *J. Non-crys. Sol.* 357, 2816 (2011). https://doi.org/10.1016/j.jnoncrysol.2011.03.006.

27. D. Toloman, R. Ciceo-Lucacel, D.A. Magdas, A. Regos, A.R. Biris, C. Leostean, and I. Ardelean, The modifier/former role of MoO₃ in some calcium-phosphate glasses. *J. Alloys Compd.* 556, 67 (2013). https://doi.org/10.1016/j.jallcom.2012.12.112.

28. L. Abbas, L. Bih, A. Nadiri, Y. El Amraoui, H. Khemakhem, and D. Mezzane, Chemical durability of MoO₃-P₂O₅ and K₂O-MoO₃-P₂O₅ glasses. *J. Ther. Analy. Calor.* 90, 453 (2007). https://doi.org/10.1007/s10973-006-7673-4.

29. A.V. Ravi Kumar, C. Srinivasa Rao, G. Murali Krishna, V. Ravi Kumar, and N. Veeraiah, Structural features of MoO₃ doped sodium sulpho borophosphate glasses by means of spectroscopic and dielectric dispersion studies. *J Mol Struct* 1016, 39 (2012). https://doi.org/10.1016/j.molstruc.2012.02.039.

30. H. Es-soufi, and L. Bih, Effect of TiO₂ on the chemical durability and optical properties of Mo-based phosphate glasses. *J. Non-Crys. Sol.* 558, 120655 (2021). https://doi.org/10.1016/j.jnoncrysol.2021.120655.

31. J. Bai, J. Hsu, R.K. Brow, C.W. Kim, J. Szabo, and A. Zervos, Structure and properties of Mo-Fe-phosphate glasses. *Eur. J. Glasses Sci. Technol. B Phys. Chem. Glasses* 60, 62 (2019). https://doi.org/10.13036/17533562.60.2.039.

32. H. Es-soufi, L. Bih, B. Manoun, and P. Lazor, Structure, thermal analysis and optical properties of lithium tungsten-titanophosphate glasses. *J. Non-Crys. Sol.* 463, 12 (2017). https://doi.org/10.1016/j.jnoncrysol.2017.02.013.

33. H.A.A. Sidek, M. Hamezan, A.W. Zaidan, Z.A. Talib, and K. Kaida, Optical characterization of lead-bismuth phosphate glasses. *Amer. J. App. Sci.* 2, 1266 (2005). https://doi.org/10.3844/ajassp.2005.1266.1269.

34. G.N. Devde, G. Upender, V. Chandra Mauli, and L.S. Ravangave, Structure, thermal and spectroscopic properties of Cᵘ²+ ions doped 59ᵦ2ᴏ3-10ₖ2O-(30–x)ZnO-xBaO-1CuO (0 ≤ x ≤ 30 mol%) glass system. *J. Non-Crys. Sol.* 432, 319 (2016). https://doi.org/10.1016/j.jnoncrysol.2015.10.022.

35. E.A. Davis, and N.F. Mott, Conduction in non-crystalline systems V Conductivity, optical absorption and photoconductivity

in amorphous semiconductors. *Phil. Mag.* 22, 903 (1970). https://doi.org/10.1080/14786437008221061.

36. M.A. Ouis, M.A. Azooz, and H.A. El Batal, Optical and infrared spectral investigations of cadmium zinc phosphate glasses doped with WO_3 or MoO_3 before and after subjecting to gamma irradiation. *J. Non-Crys. Sol.* 494, 31 (2018). https://doi.org/10.1016/j.jnoncrysol.2018.04.053.

37. J.A. Duffy, Trends in energy gaps of binary compounds: an approach based upon electron transfer parameters from optical spectroscopy. *J. Phy. C: Sol. State Phys.* 13, 2979 (1980). https://doi.org/10.1088/0022-3719/13/16/008.

38. J.A. Duffy, and M.D. Ingram, An interpretation of glass chemistry in terms of the optical basicity concept. *J. Non-Crys. Sol.* 21, 373 (1976). https://doi.org/10.1016/0022-3093(76)90027-2.

39. R.R. Reddy, Y.N. Ahammed, P.A. Azeem, K.R. Gopal, and T.V.R. Rao, Electronic polarizability and optical basicity properties of oxide glasses through average electronegativity. *J. Non-crys. Sol.* 286, 169 (2001). https://doi.org/10.1016/S0022-3093(01)00481-1.

40. H. Es-soufi, H. Bih, L. Bih, M. Azrour, B. Manoun, and P. Lazor, Structure and some physical properties of sodium ion conducting glasses inside the Na2O-Na2WO4-TiO2-P2O5 system. *J. App. Surf. Interf.* 4, 1 (2018).

41. H.A. Abo-Mosallam and E.A. Mahdy, Synthesis and characterization of sodium calcium fluorophosphate glasses containing MoO_3 for potential use in sealing applications. *J Non-Cryst Sol* 546, 120279 (2020). https://doi.org/10.1016/j.jnoncrysol.2020.120279.

42. E. Haily, L. Bih, A. El Bouari, A. Lahmar, M. El Marssi, and B. Manoun, Structural, optical, and dielectric properties of the $BaO–TiO_2–P_2O_5$ glasses. *J. Aus. Cer. Soc.* 56, 1467 (2020). https://doi.org/10.1007/s41779-020-00473-1.

43. Y. Wang, F. Wang, J. Zhou, H. Zhu, Q. Liao, L. Li, and J. Zhang, Effect of molybdenum on structural features and thermal properties of iron phosphate glasses and boron-doped iron phosphate glasses. *J. Allo. Comp.* 826, 154225 (2020). https://doi.org/10.1016/j.jallcom.2020.154225.

44. A. Dolgonos, T.O. Mason, and K.R. Poeppelmeier, Direct optical band gap measurement in polycrystalline semiconductors: a critical look at the Tauc method. *J. Sol. State Chem.* 240, 43 (2016). https://doi.org/10.1016/j.jssc.2016.05.010.

45. J.A. Duffy and M.D. Ingram, Establishment of an optical scale for Lewis basicity in inorganic oxyacids, molten salts, and glasses. *J. Amer. Chem. Soc.* 93, 6448 (1971). https://doi.org/10.1021/ja00753a019.

46. J.A. Duffy, M.D. Ingram, and I.D. Sommerville, Acid–base properties of molten oxides and metallurgical slags. *J. Chem. Soc. Far. Transactions 1: Phys. Chem. Cond. Phas.* 74, 1410 (1978). https://doi.org/10.1039/F19787401410.

47. A. Klonkowski, Bond character and properties of the mixed alkali system $Na_2O-K_2O-Al_2O_3-SiO_2$. *J. Non-Crys. Sol.* 57, 339 (1983). https://doi.org/10.1016/0022-3093(83)90064-9.

48. C.K. Jørgensen, Chemical bonding inferred from visible and ultraviolet absorption spectra. *Sol. State Phys.* 13, 375 (1962). https://doi.org/10.1016/S0081-1947(08)60460-9.

49. R. El-Mallawany, The optical properties of tellurite glasses. *J. App. Phys.* 72, 1774 (1992). https://doi.org/10.1063/1.351649.

50. E.A. Moelwyn-Hughes, *Phys. Chem.*, Vol. II (1961)

51. H. Rawson, Glass science and technology. *Proper. Appl. Glass*, 3 (1980)

52. C. Wert, C.J. Altstetter, J.O. Nelson and M.S. Rashid, The role of strain in the nucleation of solid state transformations. Illinois univ. urbana (1964)

53. A. Yariv, P. Yeh, Optical waves in crystals (Vol. 5) (1984). New York: Wil. http://mipd.snu.ac.kr

54. A.R. West, Solid state chemistry and its applications. John Wiley & Sons (2014)

55. S.R. Marder, J. E. Sohn, G. D. Stucky, Materials for nonlinear optics chemical perspectives. Amer. Chem. Soc. Wash. DC (1991)

56. V.V. Dimitrov, S.N. Kim, T. Yoko, and S. Sakka, Third harmonic generation in $PbO-SiO_2$ and $PbO-B_2O_3$ glasses. *J. Cera. Soc. Jap.* 101, 59 (1993). https://doi.org/10.2109/jcersj.101.59.

57. M. Nagarjuna, T. Satyanarayana, V.R. Kumar, and N. Veeraiah, Ag concentration dependent transport properties of glasses. *Physica B: Condensed Matter* 404, 3748 (2009). https://doi.org/10.1016/j.physb.2009.06.123.

58. L. Bih, L. Abbas, A. Nadiri, H. Khemakhem, and B. Elouadi, Investigations of molybdenum redox phenomenon in $Li_2O–MoO_3–P_2O_5$ phosphate glasses. *J. Mol. Str.* 872, 1 (2008). https://doi.org/10.1016/j.molstruc.2007.02.005.

59. M.V.R. Rao, Y. Gandhi, L.S. Rao, G. Sahayabaskaran, and N. Veeraiah, Electrical and spectroscopic properties of $LiF–Bi_2O_3–P_2O_5$: TiO_2 glass system. *Mater. Chem. Phys.* 126, 58 (2011). https://doi.org/10.1016/j.matchemphys.2010.12.010.

60. J. Cheng, G. Tilloca, and J. Zarzycki, Infra-red transmitting glass-ceramics of the As-Ge-Se system nucleated by zirconium selenide. *J. Mat. Sci.* 16, 2531 (1981). https://doi.org/10.1007/BF01113593.

61. Z. Černošek, M. Chládková, and J. Holubová, The influence of TiO_2 on the structure and properties of sodium-zinc phosphate glasses. *J. Non-Cryst. Sol.* 531, 119866 (2020). https://doi.org/10.1016/j.jnoncrysol.2019.119866.

62. M. Ganguli and K.J. Rao, Studies of ternary $Li_2SO_4–Li_2O–P_2O_5$ glasses. *J. Non-Cryst. Solids* 243, 251 (1999). https://doi.org/10.1016/S0022-3093(98)00832-1.

63. H. Segawa, N. Akagi, T. Yano, and S. Shibata, Properties and structures of $TiO_2–ZnO–P_2O_5$ glasses. *J. Ceram. Soc. Jpn.* 118, 278 (2010). https://doi.org/10.1007/BF01113593.

64. D.R. Lide ed., *CRC handbook of chemistry and physics*. (Boca Raton: CRC Press, 2001).

65. C.S. Rao, K. Seshulatha, Y.S. Gurupria, P. Sagar, M. Vijay-Kumar, S. SaibabaVali, and S. Kotireddy, Optical properties of $Na_2SO_4–B_2O_3–P_2O_5$ glasses doped with TiO2. *Mat Today: Proc.* 5, 26217 (2018). https://doi.org/10.1016/j.matpr.2018.08.070.

66. H. Gao, T. Tan, and D. Wang, Effect of composition on the release kinetics of phosphate controlled release glasses in aqueous medium. *J. Control. Release* 96, 21 (2004). https://doi.org/10.1016/j.jconrel.2003.12.030.

67. D. Ilieva, B. Jivov, G. Bogachev, C. Petkov, I. Penkov, and Y. Dimitriev, Infrared and Raman spectra of $Ga_2O_3–P_2O_5$ glasses. *J. Non-Cryst. Solids* 283, 195 (2001). https://doi.org/10.1016/S0022-3093(01)00361-1.

68. J.A. Wilder and J.E. Shelby, Property variation in alkali alkaline-earth metaphosphate glasses. *J. Am. Ceram. Soc.* 67, 438 (1984). https://doi.org/10.1111/j.1151-2916.1984.tb19732.x.

69. P. Lopez-Iscoa, L. Petit, J. Massera, D. Janner, N.G. Boetti, D. Pugliese, D. Milanese, Effect of the addition of Al_2O_3, TiO_2 and ZnO on the thermal, structural and luminescence properties of Er^{3+}-doped phosphate glasses. *J. Non-Cryst. Solids* 460, 161 (2017). https://doi.org/10.1016/j.jnoncrysol.2017.01.030.

70. G. Laudisio, M. Catauro, A. Aronne, and P. Pernice, Glass transition temperature and devitrification behaviour of lithium-titanium-germanate glasses. *Thermochim. Acta* 294, 173 (1997). https://doi.org/10.1016/S0040-6031(97)00003-8.

71. J.J. Hudgens and S.W. Martin, Glass transition and infrared spectra of low-alkali, anhydrous lithium phosphate glasses. *J. Amer. Ceram. Soci.* 76, 1691 (1993). https://doi.org/10.1111/j.1151-2916.1993.tb06636.x.

72. M. Azmoonfar, M.H. Hekmat-Shoar, and M. Mirzayi, Optical properties of glasses in the Li_2O–MoO_3–P_2O_5 system. *Ionics* 15, 513 (2009). https://doi.org/10.1007/s11581-008-0299-8.

73. B.V.R. Chowdari, R. Gopalakrishnan, S.H. Tang, and M.H. Kuok, Characterization of Ag_2O: MoO_3: P_2O_5 glasses. *Sol. State Ion.* 28–30, 704 (1988). https://doi.org/10.1016/S0167-2738(88)80128-0.

74. L. Koudelka, I. Rosslerova, J. Holubova, P. Mosner, L. Montagne, and B. Revel, Structural study of PbO–MoO_3–P_2O_5 glasses by Raman and NMR spectroscopy. *J. Non-Cryst. Solids* 357, 2816 (2011). https://doi.org/10.1016/j.jnoncrysol.2011.03.006.

75. M.A. Karakassides, A. Saranti, and I. Koutselas, Preparation and structural study of binary phosphate glasses with high calcium and/or magnesium content. *J. Non-Crys. Solids* 347, 69 (2004). https://doi.org/10.1016/j.jnoncrysol.2004.08.111.

76. A.M.B. Silva, R.N. Correia, J.M.M. Oliveira, and M.H.V. Fernandes, Structural characterization of TiO_2–P_2O_5–CaO glasses by spectroscopy. *J. Eur. Ceram. Soc.* 30, 1253 (2010). https://doi.org/10.1016/j.jeurceramsoc.2009.11.001.

77. F. Wang, M. Lu, Q. Liao, Y. Wang, H. Zhu, G. Xiang, L. Li, and Y. Zhu, Titanium-doped iron phosphate based glass ceramic waste forms containing 50 wt% simulated nuclear waste. *Mat. Chem. Phys.* 239, 122314 (2020). https://doi.org/10.1016/j.matchemphys.2019.122314.

78. D.S. Brauer, N. Karpukhina, R.V. Law, and R.G. Hill, Effect of TiO_2 addition on structure, solubility and crystallisation of phosphate invert glasses for biomedical applications. *J. Non-crys. Solids* 356, 2626 (2010). https://doi.org/10.1016/j.jnoncrysol.2010.03.022.

79. H. Es-Soufi, L. Bih, and M. Benzineb, Study of tungsten phosphate glasses containing Fe_2O_3. *New J. Glass Ceram.* 33–49, 9 (2019). https://doi.org/10.4236/njgc.2019.93004.

80. R.K. Brow, D.R. Tallant, W.L. Warren, A. Mclntyre, and D.E. Day, Spectroscopic studies of the structure of titanophosphate and calcium titanophosphate glasses. *Phys. Chem. Glasses* 300–306, 38 (1997).

81. S. Krimi, A. El Jazouli, L. Rabardel, M. Couzi, I. Mansouri, and G. Le Flem, Glass formation in the Na_2O–TiO_2–P_2O_5 system. *J. Solid State Chem.* 400–407, 102 (1993). https://doi.org/10.1006/jssc.1993.1051.

82. L. Montagne, G. Palavit, A. Shaim, M. Et-Tabirou, P. Hartmann, and C. Jager, Structure and ionic conductivity of sodium titanophosphate glasses. *J. Non-Cryst. Solids* 293–295, 719 (2001). https://doi.org/10.1016/S0022-3093(01)00783-9.

83. M. Navarro, M.P. Ginebra, J. Clément, S. Martinez, G. Avila, and J.A. Planell, Physicochemical degradation of titania-stabilized soluble phosphate glasses for medical applications. *J. Amer. Ceram. Soci.* 86, 1345 (2003). https://doi.org/10.1111/j.1151-2916.2003.tb03474.x.

84. D.S. Brauer, Bioactive glasses-structure and properties. *Angew. Chem. Int. Ed.* 54, 4160 (2015). https://doi.org/10.1002/anie.201405310.

85. A. Kiani, N.J. Lakhkar, V. Salih, M.E. Smith, R.J. Newport, D.M. Pickup, and J.C. Knowles, Titanum containing bioactive phosphate glasses. *Philos. Trans. R Soc. A* 370, 1352 (2012). https://doi.org/10.1098/rsta.2011.0276.

86. E.A. Abou Neel, W. Chrzanowski, and J.C. Knowles, Effect of increasing titanium dioxide content on bulk and surface properties of phosphate-based glasses. *Acta Biomater.* 4, 523 (2008). https://doi.org/10.1016/j.actbio.2007.11.007.

87. T. Kasuga, and Y. Abe, Calcium phosphate invert glasses with soda and titania. *J. Non-Cryst Solids* 243, 70 (1999). https://doi.org/10.1016/S0022-3093(98)00820-5.

88. J.W. Dufty, C.S. Kim, M. Bonitz, and R. Binder, Density matrix methods for semiconductor Coulomb dynamics. *Inter. J. Quant. Chem.* 65, 929 (1997).

89. D. Ehrt, P. Ebeling, and U. Natura, UV Transmission and radiation-induced defects in phosphate and fluoride–phosphate glasses. *J. Non-Cryst. Solids* 263–264, 240 (2000). https://doi.org/10.1016/S0022-3093(99)00681-X.

90. F.H. El Batal, S. Ibrahim, and M.A. Et Marzouk, UV–visible, infrared absorption spectra of undoped and TiO_2-doped lead phosphate glasses and the effect of gamma irradiation. *Rad. Effe. Defec. Solids* 167, 256 (2012). https://doi.org/10.1080/10420150.2011.637170.

91. F. Urbach, The long-wavelength edge of photographic sensitivity and of the electronic absorption of solids. *Phys. Rev.* 92, 1324 (1953). https://doi.org/10.1103/PhysRev.92.1324.

92. A.M. Ibrahim, Structural, optical and electrical investigation of sodium phosphate glasses doped MoO_3 for high power visible laser safety. *Mater. Chem. Phys.* 252, 123237 (2020). https://doi.org/10.1016/j.matchemphys.2020.123237.

93. N. Rajya Lakshmi and S. Cole, Influence of MoO_3 ions on spectroscopic properties of B_2O_3-ZnF_2-CaF_2-Al_2O_3 oxyfluoride glasses. *Mater Today: Proc.* 5, 26346–26355 (2018). https://doi.org/10.1016/j.matpr.2018.08.086.

94. A. Goldstein, V. Chiriac, and D. Becherescu, On some d 1 ions spectra in oxide glasses. *J. Non-Cryst. Solids* 92, 271 (1987). https://doi.org/10.1016/S0022-3093(87)80044-3.

95. D. Toloman, R. Suciu, C. Leostean, A. Regos, and I. Ardelean, The influence of TiO_2 concentration in some calcium-phosphate glasses. *Physica B* 438, 84 (2014). https://doi.org/10.1016/j.physb.2014.01.005.

96. M. Kaur, A. Singh, V. Thakur, and L. Singh, Effect of TiO_2 substitution on optical and structural aspects of phosphate glasses. *J. Mol. Struct.* 1089, 95 (2015). https://doi.org/10.1016/j.molstruc.2015.02.012.

97. P.G. Prakash and J.L. Rao, Cu^{2+} ions in sodium fluoride-sodium borate glasses studied by EPR and optical absorption techniques. *J. Mater. Sci.* 39, 193 (2004). https://doi.org/10.1023/B:JMSC.0000007744.87123.ee.

98. B. Tiwari, V. Sudarsan, A. Dixit, and G.P. Kothiyal, Effect of TiO_2 addition on the optical, thermo-physical, and structural aspects of sodium alumino-phosphate glasses. *J. Amer. Ceram Soci.* 94, 1440 (2011). https://doi.org/10.1111/j.1551-2916.2010.04292.x.

99. V.R. Kumar, G.N. Raju, S.V.G.V.A. Prasad, P.R. Rao, and N.N. Rao, Effect of Doping Ti^{3+} Ions on Spectroscopic Behavior of Lead Bismuth Phosphate Glasses. *Int. J. Sci. Res.* 34, 19 (2014). (**ISSN (Online): 2319-7064**).

100. H.A. El Batal, Z.E. El Mandouh, H.A. Zayed, S.Y. Marzouk, G.M. Elkomy, and A. Hosny, Gamma rays interaction with copper doped lithium phosphate glasses. *J. Molec. Struct.* 1054, 57 (2013). https://doi.org/10.1016/j.molstruc.2013.09.022.

101. W. Stambouli, H. Elhouichet, and M. Ferid, Study of thermal, structural and optical properties of tellurite glass with different TiO_2 composition. *J. Molec. Struct.* 1028, 39 (2012). https://doi.org/10.1016/j.molstruc.2012.06.027.

102. A. Moustaghfir, *Élaboration et caractérisation de couches minces d'oxyde de zinc* (Application à la photoprotection du polycarbonate: Thèse Université de Toulouse, 1997).

103. C.C. Ding, S.Y. Wu, L.N. Wu, L.J. Zhang, L. Peng, M.H. Wu, and B.H. Teng, Theoretical study of the local structures and the EPR parameters for RLNKB glasses with VO^{2+} and Cu^{2+} dopants. *J. Phys. Chem. Solids* 113, 102 (2018). https://doi.org/10.1016/j.jpcs.2017.10.012.

104. H. Es-soufi, Elaboration et caractérisations structurale, optique et électrique des verres phosphatés A_2O-A_2MO_4-TiO_2-P_2O_5

(A= Li, Na; M= Mo, W), thèse Université Moulay Ismail, 2018

105. G. Upender, S. Ramesh, M. Prasad, V.G. Sathe, and V.C. Mouli, Optical band gap, glass transition temperature and structural studies of (100–2x) TeO2–xAg2O–xWO3 glass system. *J. Alloy. Comp.* 504, 468 (2010). https://doi.org/10.1016/j.jallcom.2010.06.006.

Authors and Affiliations

H. Es-soufi[1,2] · **L. Bih**[1,3]

✉ H. Es-soufi
hichamessoufi@gmail.com

1 Equipe de Physico-Chimie de la Matière Condensée, PCMC, Faculté des Sciences de Meknès, Université Moulay Ismail, Meknes, Morocco

2 Ecole Supérieure de Génie Civil et des Nouvelles Technologies, Avenue Moulay Idriss II RUE KIFA No 38 V.N, 50003 Meknès, Morocco

3 Département matériaux et procédés, ENSAM Meknès, Université Moulay Ismail, Meknes, Morocco